PATTERN TRANSITION IN SPACECRAFT FORMATION FLYING VIA THE ARTIFICIAL POTENTIAL FIELD METHOD AND BIFURCATION THEORY

Derek J. Bennet and Colin R. McInnes

Department of Mechanical Engineering, University of Strathclyde, Glasgow, Scotland, G1 1XJ,
{derek.bennet,colin.mcinnes}@strath.ac.uk

1. ABSTRACT

In recent years many new and exciting space concepts have developed around spacecraft formation flying. This form of distributed system has the advantages of being extremely flexible and robust. This paper considers the development of new control methodologies based on the artificial potential function method and extends previous research in this area by considering bifurcation theory as a means of controlling the transition between different formations. For real, safety critical applications it is important to prove the stability of the system. This paper therefore aims to replace algorithm validation with mathematical proof through dynamical systems theory. Finally we consider the transition of formations at the Sun-Earth L_2 point.

2. INTRODUCTION

In recent years formation flying has emerged as an important type of distributed satellite system that enables a variety of missions that can improve significantly the functionality of the system in comparison with a large single satellite [1]. Gill et al. [2] define formation flying "*as a technology, that includes two or more spacecraft in a tightly controlled spatial configuration, whose operations are closely synchronized*". This technology can then be used to create a single virtual sensor much larger than what could be achieved with a single satellite.

At present there are several formation flying concepts that are being investigated. NASA, for example, have been studying the use of formation flying for interferometric/sparse aperture missions. The Stellar Imager is an example of such a mission that consists of a UV/Optical deep-space telescope composed of approximately 30 one-meter array elements [3]. Another example is ESA's DARWIN mission that will consist of 6 spacecraft equipped with telescopes, searching for earth-like planets [4].

The distributed control of spacecraft flying in formation can be divided into either centralised or decentralised control. Landsat-7 and Earth Observing-1 satellites are examples of a hierarchical (leader-follower) centralised mission and is generally considered the first real mission to demonstrate formation flying. The two satellites in this formation do not communicate with each other and are controlled discretely by the ground. The limitation of this system is that it is dependent upon the central controller and is therefore susceptible to failure. As the number of spacecraft increase, the workload required to maintain a formation discretely will increase significantly. A promising approach to overcome this is to develop control architectures based on an autonomous decentralised system in which all spacecraft interact producing an emergent behaviour. For example, McQuade et al. have shown how this can be achieved in the autonomous configuration of satellite formations [5] through the use of an artificial potential function method.

The aim of this paper to develop new control methodologies for formation flying missions, taking inspiration from the work done in behavioral robotics. In addition it also considers increasing the formation size (>10), being able to switch between different formations through a simple parameter change and verifying through dynamical systems theory that desired behaviors will always occur.

Behavioural Robotics was first introduced in the mid $1980's$ by Brooks [6] who suggested that although previous research had been dominated by the ideas of a centralised control paradigm, a significant step forward would be to draw on inspiration from nature and have a decentralised control system.

There are several different control architectures in behavioral robotics with one of the most popular being based on the superposition architecture [7] such as the artificial potential function method used throughout this paper. It has been used successfully, for example, by Reif and Wang as a form

of distributed behavioral control for autonomous robots [8], by Badaway and McInnes in autonomous structure assembly [9] and by McQuade [5] for formation flying.

For real, safety critical applications it is essential that the behaviour of the spacecraft be verified in order to ensure that no unwanted behaviours will occur. Winfield [10] has introduced the term 'swarm engineering' to highlight the key issues that are involved in real, safety critical applications as opposed to those based on simulation. Through the use of dynamical systems theory this paper aims to replace algorithm validation with mathematical proof in order to control spacecraft flying in formation. Bifurcation methods are employed to create a flexible system that can allow for different configurations to be formed through a simple parameter change.

The paper proceeds as follows. In the next section we describe the model used and explain the artificial function method and bifurcation theory. Section 3 considers the stability of the system and section 4 moves on to show the different formations that can be achieved using the model. Section 5 considers the deployment of a spacecraft formation flying at the Sun-Earth Lagrangian L_2 point.

3. FORMATION MODEL

3.1. Artificial Potential Functions and Bifurcation Theory

We consider a swarm of homogeneous autonomous satellites ($1 \leq i \leq N$) interacting via an artificial potential function, U. The negative gradient of the artificial potential defines a virtual force acting on each spacecraft so the dynamics of each spacecraft can be described by Eq. 1 and 2 with mass, m, position, $\mathbf{x}_i$, and velocity, $\mathbf{v}_i$;

$$\frac{d\mathbf{x}_i}{dt} = \mathbf{v}_i \tag{1}$$

$$m\frac{d\mathbf{v}_i}{dt} = -\nabla_i U^S(\mathbf{x}_i) - \nabla_i U^R(\mathbf{x}_{ij}) - \sigma\mathbf{v}_i \tag{2}$$

From Eq. 2 it can be seen that the virtual force experienced by each satellite is dependent upon the gradient of two different artificial potential functions and a dissipative term, where $\sigma > 0$ is a constant that controls the amplitude of the dissipation. The first term in Eq. 2 is the *steering potential*, U^S, whereas the second term in Eq. 2 is the *repulsive potential*, U^R.

The *steering potential* is based on the simple pitchfork bifurcation [11] as shown in the first two terms of Eq. 3. The aim of this potential is to drive each satellite to a goal distance, r, from the origin in the x-y plane. The last term in Eq. 3 is to ensure that the formation is created in the x-y plane, where the constant α controls the amplitude of this quadratic potential and $\mathbf{x}_i = (x_i, y_i, z_i)^T$.

$$\begin{aligned} U^S(\mathbf{x}_i) &= -\frac{1}{2}\mu\left((x_i^2 + y_i^2)^{1/2} - r\right)^2 \\ &\quad + \frac{1}{4}\left((x_i^2 + y_i^2)^{1/2} - r\right)^4 + \frac{1}{2}\alpha z_i^2 \end{aligned} \tag{3}$$

Depending on the value of μ, the steering potential can have various forms. Fig. 1 shows how the potential bifurcates into the two local minima when $\mu = 0$ and Fig. 2 shows an example of the potential when μ is negative and positive.

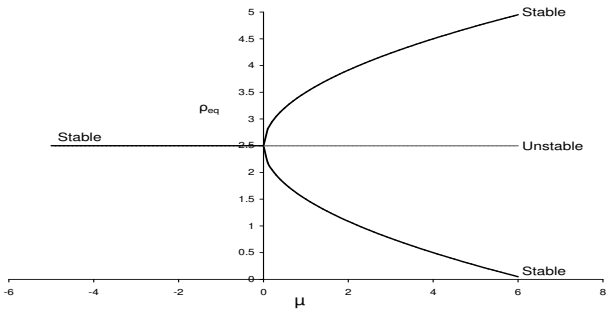

Figure 1. Pitchfork bifurcation diagram

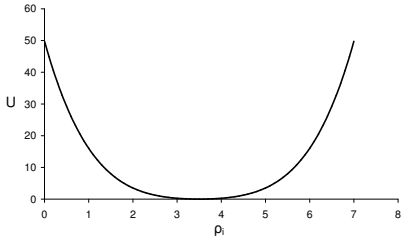

(i)

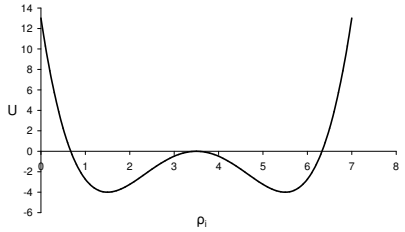

(ii)

Figure 2. Potential field: (i) $\mu < 0$ and (ii) $\mu > 0$

The stability of the equilibrium state of the artificial potential can be determined by reducing the equation to two variables, ρ_i and z_i as shown in Eq. 4, where $\rho_i = (x_i^2 + y_i^2)^{1/2}$ and $\mathbf{x}_i = (\rho_i, z_i)^T$.

$$U^S(\mathbf{x}_i) = -\frac{1}{2}\mu\left(\rho_i - r\right)^2 + \frac{1}{4}\left(\rho_i - r\right)^4 + \frac{1}{2}\alpha z_i^2 \quad (4)$$

For a function consisting of two variables the stability of the system is determined from the sign of D given in Eq. 5 [12].

$$D = \frac{\partial^2 U}{\partial \rho_i^2}\frac{\partial^2 U}{\partial z_i^2} - \left[\frac{\partial^2 U}{\partial \rho_i \partial z_i}\right] \quad (5)$$

The conditions for stability are as follows;

(i) $D > 0$, $\partial^2 U/\partial \rho_i^2 > 0 \Longrightarrow$ equilibrium point is a stable minimum.
(ii) $D > 0$, $\partial^2 U/\partial \rho_i^2 < 0 \Longrightarrow$ equilibrium point is a unstable maximum.
(iii) $D < 0 \Longrightarrow$ equilibrium point is a saddle.

The equilibrium of the potential occurs whenever $\partial U/\partial \rho_i = 0$ and $\partial U/\partial z_i = 0$. Therefore,

$$\frac{\partial U}{\partial \rho_i} = -\mu(\rho_i - r) + (\rho_i - r)^3 \quad (6)$$

$$\frac{\partial U}{\partial z_i} = \alpha z_i \quad (7)$$

If $\mu \leq 0$ equilibrium occurs when $\rho_i = r$. If $\mu > 0$ equilibrium occurs when $\rho_i = r$, $r \pm \sqrt{\mu}$. To determine whether the equilibrium is either a stable minimum or unstable maximum we have to consider the sign of the second derivative of the potential shown in Eq. 8 and Eq. 9.

$$\frac{\partial^2 U}{\partial \rho_i^2} = -\mu + 3(\rho_i - r)^2 \quad (8)$$

$$\frac{\partial^2 U}{\partial z_i^2} = \alpha \quad (9)$$

From Eq. 9 it can be seen that $\partial^2 U/\partial \rho_i \partial z_i = 0$ and as α is positive, $\partial^2 U/\partial z_i^2 > 0$.

From Eq. 8 it can be seen that $\partial^2 U/\partial \rho_i^2 \gtrless 0$ depending on the values of μ. Therefore, the properties of the equilibrium state ρ_{eq} are:

when $\mu < 0 \Longrightarrow$
$\rho_{eq} = r$, so $\partial^2 U/\partial \rho_i^2 > 0 \Longrightarrow \rho_{eq}$ is a stable minimum.
when $\mu > 0 \Longrightarrow$
$\rho_{eq} = r$, so $\partial^2 U/\partial \rho_i^2 < 0 \Longrightarrow \rho_{eq}$ is an unstable maximum.
$\rho_{eq} = r + \sqrt{\mu}$, so $\partial^2 U/\partial \rho_i^2 > 0 \Longrightarrow \rho_{eq}$ is a stable minimum.
$\rho_{eq} = r - \sqrt{\mu}$, so $\partial^2 U/\partial \rho_i^2 > 0 \Longrightarrow \rho_{eq}$ is a stable minimum.

as can be seen in Fig. 1 and Fig. 2.

The *repulsive potential* is based on a generalized Morse Potential [13] as shown in Eq. 10.

$$U_{ij}^R = \sum_{j, j \neq i} C_r \exp^{-|\mathbf{x}_{ij}|/L_r} \quad (10)$$

Where the constants C_r and L_r represent the amplitude and range of repulsive potential respectively and $\mathbf{x}_{ij} = \mathbf{x}_i - \mathbf{x}_j$. The total repulsive force on the i^{th} spacecraft is dependent upon the position of all the other $(N-1)$ satellites in the swarm.

The repulsive potential is therefore used to ensure that as the spacecraft are steered towards the goal state they do not collide with each other. Once all the spacecraft have been driven to the desired equilibrium state the repulsive potential also ensures that they are equally spaced in a ring.

3.2. Cusp Catastrophe

A useful extension to the 1D pitchfork bifurcation is to consider the 2D Cusp Catastrophe given in Eq. 11. Fig. 3 shows the variation of the equilibrium position with the two parameters, μ and v.

$$U(\rho_i; \mu, v) = \mu\left(\rho_i - r\right)^2 + \left(\rho_i - r\right)^4 + v(\rho_i - r) \quad (11)$$

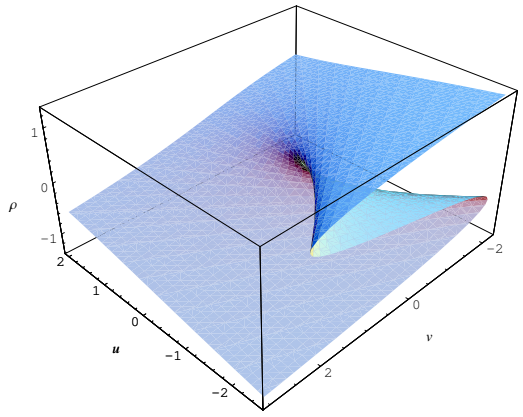

Figure 3. Cusp catastrophe surface [14]

For the cusp potential, if we set v equal to zero we have the usual pitchfork bifurcation equation as shown in Fig. 4. If however, $v > 0$ and $v < 0$ the system can be tipped into either the lower or upper branch of the pitchfork equation as shown in Fig. 5. Thus if the system was in the bi-stable state, control over the position of a single minima state can be achieved through the variation of the 2D bifurcation parameters.

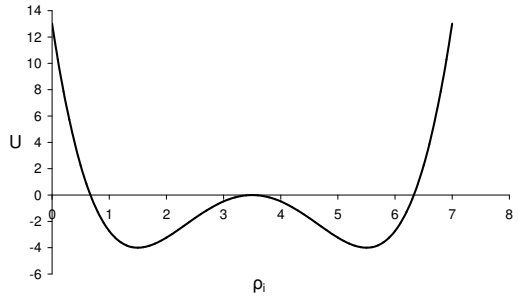

Figure 4. Bi-stable state: two ringed formation $v = 0$, $\mu < 0$

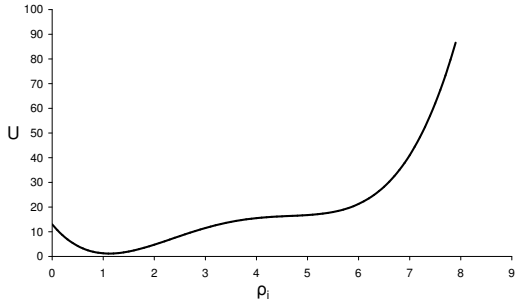

(i)

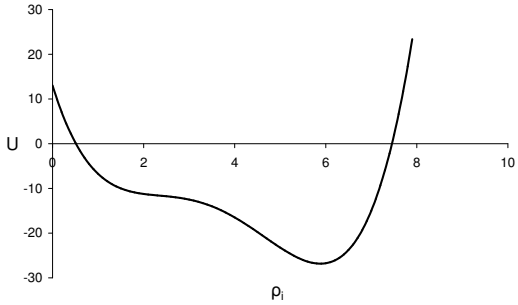

(ii)

Figure 5. Potential field: (i) $v < 0$ and (ii) $v > 0$

3.3. Rotation of Formation

Recent work by McInnes [15] has shown how vortex like swarming can be achieved through artificial potential field methods. Eq. 1 and 2 are altered to include an dissipative orientation term instead of the velocity dependent dissipative term as shown in Eq. 12 and 13. Eq. 14 shows the orientation term that dissipates energy whilst aligning the velocity vectors of members of the swarm where C_o and L_o are constants.

$$\frac{d\mathbf{x}_i}{dt} = \mathbf{v}_i \tag{12}$$

$$m\frac{d\mathbf{v}_i}{dt} = -\Lambda_i - \nabla_i U^S(\mathbf{x}_i) - \nabla_i U^R(\mathbf{x}_{ij}) \tag{13}$$

$$\Lambda_i = \sum_{i \neq j} C_o(\mathbf{v}_{ij}.\hat{\mathbf{x}}_{ij} \exp^{|\mathbf{x}_{ij}|/l_o})\hat{\mathbf{x}}_{ij} \tag{14}$$

The vortex like results can be seen through the conservation of angular momentum. Taking the cross product of the Eq. 13 with the position vector, $\mathbf{x}_i$, the conservation of angular momentum can be seen since $\mathbf{x}_i \times \mathbf{x}_i = 0$ by definition and the sum of $\mathbf{x}_i \times \mathbf{x}_j$ vanishes since $\mathbf{x}_i \times \mathbf{x}_j = -(\mathbf{x}_j \times \mathbf{x}_i)$ so that;

$$\begin{aligned} \mathbf{x}_i \times -\Lambda_i &= \sum_{i \neq j} C_o \left(\mathbf{v}_{ij}.\frac{(\mathbf{x}_i \times \mathbf{x}_i - \mathbf{x}_i \times \mathbf{x}_j)}{|\mathbf{x}_{ij}|} \right) \\ &\quad \exp^{|\mathbf{x}_{ij}|/l_o} \hat{\mathbf{x}}_{ij} \\ &= 0 \end{aligned} \tag{15}$$

$$\begin{aligned} \mathbf{x}_i \times -\nabla_i U^S(\mathbf{x}_i) &= \mu\frac{\mathbf{x}_i \times \mathbf{x}_i}{|\mathbf{x}_i|}(|\mathbf{x}_i| - r) \\ &\quad -\frac{\mathbf{x}_i \times \mathbf{x}_i}{|\mathbf{x}_i|}(|\mathbf{x}_i| - r)^3 \\ &= 0 \end{aligned} \tag{16}$$

$$\begin{aligned} \mathbf{x}_i \times -\nabla_i U^R(\mathbf{x}_{ij}) &= -\sum_{i \neq j} \frac{C_r}{L_r} \exp^{-|\mathbf{x}_{ij}|/L_r} \\ &\quad \frac{(\mathbf{x}_i \times \mathbf{x}_i - \mathbf{x}_i \times \mathbf{x}_j)}{|\mathbf{x}_{ij}|} \\ &= 0 \end{aligned} \tag{17}$$

The rate of change of angular momentum ($\mathbf{H}$) can therefore be shown to equal zero by summing over all states as shown in Eq. 18, so that the system conserves angular momentum.

$$\begin{aligned} \sum_i \mathbf{x}_i \times m\dot{\mathbf{v}}_i &= \frac{d}{dt}\sum_i (\mathbf{x}_i \times m\mathbf{v}_i) \\ &= \frac{d\mathbf{H}}{dt} = 0 \end{aligned} \tag{18}$$

The swarm therefore dissipates energy while conserving angular momentum and so relaxes into the rotating ring [15].

3.4. Orientation of Formation

So far the dynamical equations have been set up in order for the formation to be created in the x-y plane. It may however be required to create the formation in a different plane and this can be achieved through the direction cosine matrix approach [16].

Rotating about the x-axis and y-axis by an angle of α and β respectively we can achieve different orientations of the formation. The direction cosine matrix, $\mathbf{C}$, for each rotation about the x and y axis is shown in Eq. 19 and 20.

$$\mathbf{C}_x = \begin{pmatrix} 1 & 0 & 0 \\ 0 & Cos\alpha & Sin\alpha \\ 0 & -Sin\alpha & Cos\alpha \end{pmatrix} \tag{19}$$

$$\mathbf{C}_y = \begin{pmatrix} Cos\beta & 0 & -Sin\beta \\ 0 & 1 & 0 \\ Sin\beta & 0 & Cos\beta \end{pmatrix} \tag{20}$$

The new desired position vector, $\mathbf{x}'_i$, is therefore shown in Eq. 21.

$$\begin{bmatrix} x'_i \\ y'_i \\ z'_i \end{bmatrix} = \mathbf{C}_x\mathbf{C}_y \begin{bmatrix} x_i \\ y_i \\ z_i \end{bmatrix} \tag{21}$$

4. STABILITY

In order to use the methods developed in real, safety critical applications it is important that the stability of the system be determined to ensure that desired behaviours will always occur. As real engineered systems are often subject to noise, it is important to ensure that system will remain in the desired configuration even if it is perturbed. To determine the stability of our system we consider two methods; Lyapunov's Second Theorem and an eigenvalue analysis of the linearized equations of motion.

4.1. Non-linear Stability

To determine the non-linear stability of the dynamical system, Lyapunov's Second Theorem can be used as expressed by Kalman and Bertram [17][18];

"*If the rate of change of* $dE(\boldsymbol{x})/dt$ *of the energy* $E(\boldsymbol{x})$ *of an isolated physical system is negative for every possible state* $\boldsymbol{x}$*, except for a single equilibrium state* $\boldsymbol{x}_e$*, then the energy will continually decrease until it finally assumes its minimum value* $E(\boldsymbol{x}_e)$"

The aim of the *steering potential* is to drive the spacecraft to the desired equilibrium position that corresponds to the minimum of artificial potential. Therefore, if Lyapunov's Second Method can be proved for the system, as time evolves the system will relax into the minimum energy state.

The Lyapunov function, L, is defined as the total energy of the system, where $U^S(\mathbf{x}_i)$ and $U^R(\mathbf{x}_{ij})$ are defined in Eq. 3 and Eq. 10 respectively so that;

$$L = \sum_i \left(\frac{1}{2}\mathbf{v}_i^2 + U^S(\mathbf{x}_i) + U^R(\mathbf{x}_{ij}) \right) \tag{22}$$

It should be noted that since the *repulsive potential* is a pairwise force, the summation over the entire system will vanish ($\sum_i \nabla_i U^R(\mathbf{x}_{ij}) = 0$).

The rate of change of the Lyapunov function can be expressed as;

$$\frac{dL}{dt} = \left(\frac{\partial L}{\partial \mathbf{x}_i} \right) \dot{\mathbf{x}}_i + \left(\frac{\partial L}{\partial \mathbf{v}_i} \right) \dot{\mathbf{v}}_i \tag{23}$$

Then, substituting Eq. 2 into Eq. 23 it can be seen that;

$$\frac{dL}{dt} = -\sum_i \sigma \mathbf{v}_i^2 \leq 0 \tag{24}$$

From [11] Lyapunov's Second Theorem states that if L is a positive definite and $\dot{L}$ is a negative definite the system will be uniformly stable. A problem arises in the use of the superimposed artificial potential function as $\dot{L} \leq 0$. This implies that $\dot{L}$ could equal zero in a position other than the goal minimum suggesting that the system may become trapped in a local minimum. In order to ensure that our system is asymptotically stable at the desired goal state the LaSalle principle [19] can be used. It extends the above constraints to state that if $L(0) = \dot{L}(0) = 0$ and the set $\{\mathbf{x}_i | \dot{L} = 0\}$ only occurs when $\mathbf{x}_i = \mathbf{x}_{eq}$, then the goal state is asymptotically stable. Therefore, for the dynamic system considered in this paper the LaSalle principle is valid. As we have a well defined symmetric potential field, equilibrium only occurs at the goal state so the local minima problem can be avoided and the system will relax into the desired goal configuration.

4.2. Linear Stability

The purpose of the linear stability analysis is to determine the local behaviour of the system by calculating its eigenvalue spectrum. Therefore, by neglecting the repulsive potential, equilibrium of Eq. 1 and 2 occurs when $\dot{\mathbf{x}}_i = \dot{\mathbf{v}}_i = 0$, so $\mathbf{v}_i = 0$ and $\nabla U^S = 0$. This occurs when $\rho_{eq} = r$ if $\mu < 0$ and $\rho_{eq} = r, r \pm \sqrt{\mu}$ if $\mu > 0$, with $z_{eq} = 0$.

By considering small displacements from the equilibrium points of the system, linearisation can be used to predict the system behaviour such that;

$$\begin{pmatrix} \dot{\mathbf{x}}_i \\ \dot{\mathbf{v}}_i \end{pmatrix} = \begin{pmatrix} \mathbf{v}_i \\ -\sigma \mathbf{v}_i - \nabla_i U^S(\mathbf{x}_i) \end{pmatrix} = \begin{pmatrix} f(\mathbf{x}_i, \mathbf{v}_i) \\ g(\mathbf{x}_i, \mathbf{v}_i) \end{pmatrix} \tag{25}$$

Let $\mathbf{x}_o$ and $\mathbf{v}_o$ denote fixed points with $\dot{\mathbf{x}}_i = \dot{\mathbf{v}}_i = 0$ so that;

$$f(\mathbf{x}_o, \mathbf{v}_o) = 0 \tag{26}$$

$$g(\mathbf{x}_o, \mathbf{v}_o) = 0 \tag{27}$$

Defining $\delta\mathbf{x}_i = \mathbf{x}_i - \mathbf{x}_o$ and $\delta\mathbf{v}_i = \mathbf{v}_i - \mathbf{v}_o$ and Taylor Series expanding about the fixed points the eigenvalues of system can be found. As it is assumed that $\delta\mathbf{x}_i$ and $\delta\mathbf{v}_i$ are small, we only consider the first order terms of the expansion so that;

$$\begin{pmatrix} \delta\dot{\mathbf{x}}_i \\ \delta\dot{\mathbf{v}}_i \end{pmatrix} = \mathbf{J} \begin{pmatrix} \delta\mathbf{x}_i \\ \delta\mathbf{v}_i \end{pmatrix} \tag{28}$$

where,

$$\mathbf{J} = \begin{pmatrix} \frac{\partial}{\partial \mathbf{x}_i}(f(\mathbf{x}_i, \mathbf{v}_i)) & \frac{\partial}{\partial \mathbf{v}_i}(f(\mathbf{x}_i, \mathbf{v}_i)) \\ \frac{\partial}{\partial \mathbf{x}_i}(g(\mathbf{x}_i, \mathbf{v}_i)) & \frac{\partial}{\partial \mathbf{v}_i}(g(\mathbf{x}_i, \mathbf{v}_i)) \end{pmatrix}\Bigg|_{\mathbf{x}_o, \mathbf{v}_o} \tag{29}$$

The Jacobian, $\mathbf{J}$, is then a $4x4$ matrix given by;

$$\mathbf{J} = \begin{pmatrix} 0 & 0 & 1 & 0 \\ 0 & 0 & 0 & 1 \\ -\frac{\partial^2 U}{\partial \rho_i^2} & -\frac{\partial^2 U}{\partial \rho_i \partial z_i} & -\sigma & 0 \\ -\frac{\partial^2 U}{\partial \rho_i \partial z_i} & -\frac{\partial^2 U}{\partial z_i^2} & 0 & -\sigma \end{pmatrix}\Bigg|_{\tilde{\mathbf{x}}_o, \mathbf{v}_o} \tag{30}$$

Substituting a trial exponential solution into Eq. 28 we find that;

$$\begin{pmatrix} \delta\tilde{\mathbf{x}}_i \\ \delta\mathbf{v}_i \end{pmatrix} = \begin{pmatrix} \delta\mathbf{x}_o \\ \delta\mathbf{v}_o \end{pmatrix} e^{\lambda t} \tag{31}$$

Therefore, the eigenvalues, λ, of the system are found when $det(\mathbf{J} - \lambda\mathbf{I}) = 0$.

4.2.1. Eigenvalue Spectrum when $\mu \leq 0$

As shown previously, if $\mu \leq 0$ equilibrium of the system occurs when $\mathbf{x}_{o1} = (r, 0)$ and $\mathbf{v}_i = 0$. Evaluating the Jacobian matrix given in Eq. 30 we find that;

$$\mathbf{J}_1 = \begin{pmatrix} 0 & 0 & 1 & 0 \\ 0 & 0 & 0 & 1 \\ \mu & 0 & -\sigma & 0 \\ 0 & -\alpha & 0 & -\sigma \end{pmatrix} \tag{32}$$

The corresponding eigenvalue spectrum is therefore;

$$\lambda = \begin{cases} 1/2(-\sigma \pm \sqrt{(\sigma^2 - 4\alpha)}) \\ 1/2(-\sigma \pm \sqrt{(\sigma^2 + 4\mu)}) \end{cases} \tag{33}$$

Depending upon the values of the constants in the dynamical system, the eigenvalues can be chosen to obtain different classifications for the equilibrium. For $\mu < 0$, if the constants σ and α are chosen so that $\sigma^2 + 4\mu < 0$ and $\sigma^2 - 4\alpha < 0$, the system will be in an asymptotically stable spiral. If, however, $\mu = 0$, the eigenvalues are; $\lambda = 1/2(-\sigma \pm \sqrt{(\sigma^2 - 4\alpha)})$ and $\lambda = -\sigma; 0$ so the system will be in a stable spiral mode.

As an example consider a system with the following parameters; $\mu = -2.5$, $\alpha = 2$ and $\sigma = 2$. The corresponding eigenvalues are then; $\lambda = -1 \pm 2\mathbf{i}$ and $-1 \pm 2.45\mathbf{i}$ indicating that if a spacecraft was driven to the equilibrium state and given a small perturbation it would relax back into that equilibrium state.

4.2.2. Eigenvalue Spectrum when $\mu > 0$

If $\mu > 0$ equilibrium of the system occurs when $\mathbf{x}_{o1} = (r, 0)$, $\mathbf{x}_{o2} = (r + \sqrt{\mu}, 0)$ and $\mathbf{x}_{o3} = (r - \sqrt{\mu}, 0)$ with $\mathbf{v}_i = 0$. The Jacobian matrix evaluated at the three different equilibrium positions is given by Eq. 34, 35 and 36 respectively as;

$$\mathbf{J}_1 = \begin{pmatrix} 0 & 0 & 1 & 0 \\ 0 & 0 & 0 & 1 \\ \mu & 0 & -\sigma & 0 \\ 0 & -\alpha & 0 & -\sigma \end{pmatrix} \tag{34}$$

$$\mathbf{J}_2 = \begin{pmatrix} 0 & 0 & 1 & 0 \\ 0 & 0 & 0 & 1 \\ \mu - 3\sqrt{\mu} & 0 & -\sigma & 0 \\ 0 & -\alpha & 0 & -\sigma \end{pmatrix} \quad (35)$$

$$\mathbf{J}_3 = \begin{pmatrix} 0 & 0 & 1 & 0 \\ 0 & 0 & 0 & 1 \\ \mu + 3\sqrt{\mu} & 0 & -\sigma & 0 \\ 0 & -\alpha & 0 & -\sigma \end{pmatrix} \quad (36)$$

The eigenvalues for $\mathbf{J}_1$ are;

$$\lambda = \begin{cases} 1/2\left(-\sigma \pm \sqrt{(\sigma^2 - 4\alpha)}\right) \\ 1/2\left(-\sigma \pm \sqrt{(\sigma^2 + 4\mu)}\right) \end{cases} \quad (37)$$

Therefore, referring back to Fig. 2(ii) it can be seen that when $\mu > 0$ and $\mathbf{x}_{o1} = (r, 0)$ this should correspond to an unstable position. For this to be true the parameters in Eq. 37 have to be chosen in order for the eigenvalues to be either real and positive or complex with a positive real part.

The eigenvalues for $\mathbf{J}_2$ are;

$$\lambda = \begin{cases} 1/2\left(-\sigma \pm \sqrt{(\sigma^2 - 4\alpha)}\right) \\ 1/2\left(-\sigma \pm \sqrt{(\sigma^2 + 4\mu - 12\sqrt{\mu})}\right) \end{cases} \quad (38)$$

Again referring back to Fig. 2(ii) it can be seen that when $\mu > 0$ and $\mathbf{x}_{o2} = (r + \sqrt{\mu}, 0)$ the system should be in a stable equilibrium. To ensure that this is the case the constants have to be chosen so that the eigenvalues are either complex with negative real part or real and negative.

Lastly the eigenvalues for $\mathbf{J}_3$ are;

$$\lambda = \begin{cases} 1/2\left(-\sigma \pm \sqrt{(\sigma^2 - 4\alpha)}\right) \\ 1/2\left(-\sigma \pm \sqrt{(\sigma^2 + 4\mu + 12\sqrt{\mu})}\right) \end{cases} \quad (39)$$

Again Fig. 2(ii) indicates that this point should be stable, therefore by ensuring that the constants are chosen so that the eigenvalues are either complex with negative real part or real and negative the equilibrium position will be linearly stable.

5. NUMERICAL RESULTS

5.1. Formation Patterns

Fig. 6 shows the three different satellite formations that can be formed using the pitchfork bifurcation. The system considered is for a swarm of 30 spacecraft with unit mass, where σ and α are constant throughout the simulation.

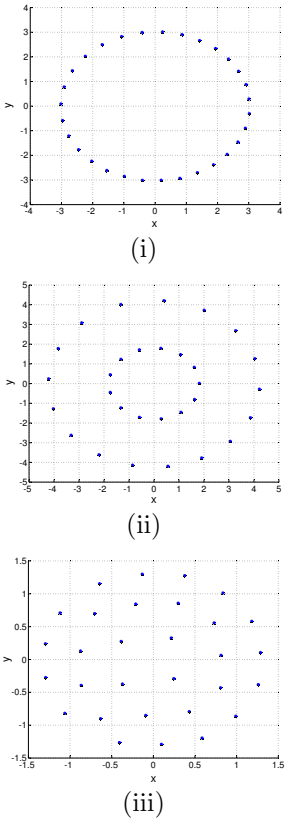

Figure 6. Formation patterns: (i) ring (ii) two rings (iii) cluster

The first formation shows a ring corresponding to $\mu = -2$. The radius of the ring is determined by the magnitude that the *steering potential* has been moved along the x-axis (in this case $r = 3$). The second formation consists of two rings, where the *steering potential* has been altered to the bi-stable state with $\mu = 2$. The stable equilibrium point in the first formation then becomes unstable and the system bifurcates into two rings. The final formation corresponds to the case when $\mu = -2$ and $r = 0$. The spacecraft are then driven towards the origin with the *repulsive potential* causing a cluster to form.

5.2. Transition between Formations

Figures 7 shows the transition of a formation of 30 spacecraft in the x-y plane. As it can be seen

from Fig. 7, the system changes from a ring to two rings to a cluster then back to a ring. This is achieved through a very simple parameter change and is one of the advantages of using the pitchfork bifurcation equation as a basis for the artificial potential function. Rather than controlling each spacecraft individually the global pattern of the formation can be manipulated by the bifurcation parameter, μ.

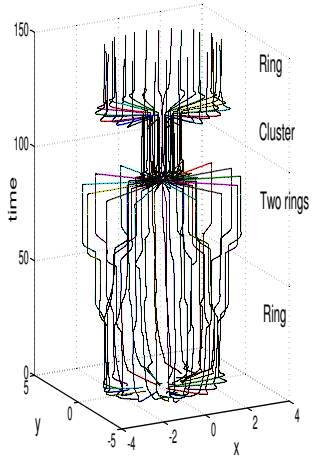

(i)

Figure 7. Smooth transition between different formations: (i) formation of the pattern on the x-y plane (ii) evolution of system in x-y plane

5.3. Cusp Catastrophe Transitions

Figure 8 demonstrates how a 2D bifurcation can be used to alter a spacecraft formation. As can be seen if we start in the two ring case when $v = 0$ and vary v therefore performing a bifurcation on the system we can either tip the system into a large or small ring.

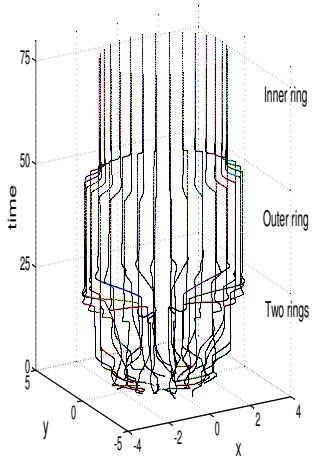

Figure 8. Evolution of cusp catastrophe results

5.4. Rotation of the Formation

Figures 9 shows the rotation of the ring formation using Eq. 14. The formation relaxes into to a single ring and conserves angular momentum by rotating about its centre of mass.

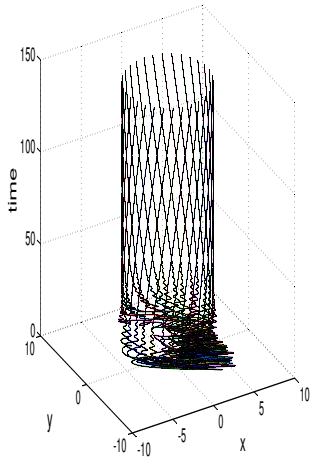

Figure 9. Time evolution of vortex ring

5.5. Orientation of the Formation

By defining the desired orientation angle different orientations of the formation of spacecraft can be achieved as shown in Fig. 10. The results show a formation of spacecraft being formed at an angle $\alpha = 45°$ and $\beta = 30°$.

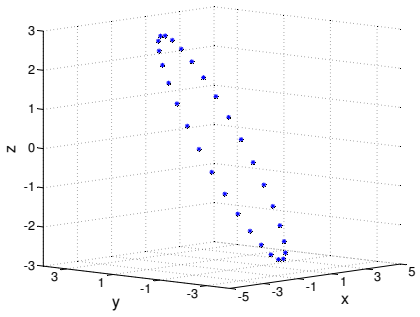

Figure 10. Orientation of formation: $\alpha = 45°$ and $\beta = 30°$

6. SUN-EARTH L_2 POINT

In this section we consider positioning a spacecraft formation at the Sun-Earth L_2 lagrange point. Using a similar convention to that set out by Wie [16] the dynamics of this system are found by considering the circular restricted three body problem. It is

assumed that the motion of the Sun and Earth are constrained to circular orbits about their barycenter and that they rotate at a constant angular velocity (ω). Fig. 11 shows the circular restricted three body problem in the rotating coordinate frame about the barycenter for the Sun and Earth.

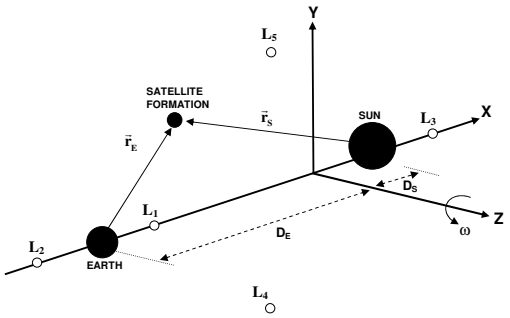

Figure 11. Sun-Earth circular restricted three body problem

For the Sun-Earth system there are five equilibrium points in the system with the collinear equilibrium points (X_0, Y_0, Z_0), occuring at $L_1(-0.990026D, 0, 0)$, $L_2(-1.01003D, 0, 0)$ and $L_3(1D, 0, 0)$ where, $D = D_s + D_e = 1.5 \times 10^{11} m$.

From Wie [16] the linearized equations of motion about the L_2 equilibrium point are described by Eq. 40, 41 and 42 assuming unit mass for each spacecraft.

$$\ddot{x}_i - 2\omega\dot{y}_i - (\omega^2 + 2\zeta^2)x_i = 0 \tag{40}$$

$$\ddot{y}_i + 2\omega\dot{x}_i + (\zeta^2 - \omega^2)y_i = 0 \tag{41}$$

$$\ddot{z}_i + \zeta^2 z_i = 0 \tag{42}$$

where,

$$\begin{aligned} \omega &= \sqrt{\left[\frac{G(M_{earth} + M_{sun})}{D^3}\right]} \\ &= 1.9830 \times 10^{-7} \text{rad/s} \end{aligned} \tag{43}$$

$$\zeta = \frac{M_{earth}}{M_{earth} + M_{sun}} = 3.0037 \times 10^{-6} \tag{44}$$

Using the linearized system centered on the L_2 point the equations of motion can be altered to include the steering, repulsive and dissipative forces defined in Eq. 2 so that the full linearized equations of motion for each spacecraft described by Eq. 45, 46 and 47 are;

$$\begin{aligned} \ddot{x}_i - 2\omega\dot{y}_i - (\omega^2 + 2\zeta^2)x_i &= -\sigma\dot{x}_i - \frac{\partial U^R}{\partial x_i} \\ &\quad - \frac{\partial U^S}{\partial x_i} \end{aligned} \tag{45}$$

$$\begin{aligned} \ddot{y}_i + 2\omega\dot{x}_i + (\zeta^2 - \omega^2)y_i &= -\sigma\dot{y}_i - \frac{\partial U^R}{\partial y_i} \\ &\quad - \frac{\partial U^S}{\partial y_i} \end{aligned} \tag{46}$$

$$\ddot{z}_i + \zeta^2 z_i = -\sigma\dot{z}_i - \frac{\partial U^R}{\partial z_i} - \frac{\partial U^S}{\partial z_i} \tag{47}$$

Figure 12 shows the evolution of the system of 30 spacecraft interacting and forming a single ring and then through the pitchfork fork bifurcation method altering to a cluster in the x-y plane.

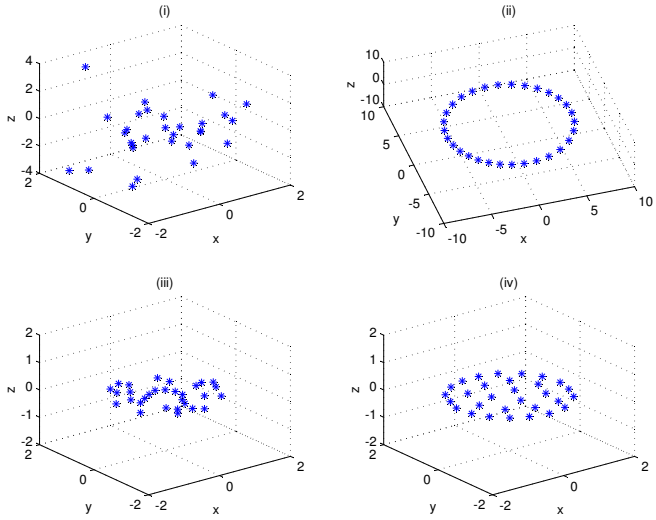

Figure 12. Spacecraft formation at L_2: (i) initial conditions (ii) formation of a single ring (iii) bifurcation of system (iv) formation of the cluster

7. CONCLUSION

We have shown that the control of spacecraft flying in formation can be achieved through the use of the artificial potential function method. We have extended previous research in this area through the use of bifurcation theory to demonstrate that through a simple parameter change a formation of spacecraft can be made to alter their configuration and shown how 1D and 2D bifurcations can be used to this effect. An important step in real engineered systems is to ensure that the formation can form reliably. Through dynamical systems theory we have proved the non-linear stability of the system and also the

linear stability of a spacecraft driven to the equilibrium position. To demonstrate the use of the method developed here in space applications the formation is established about the Sun-Earth L_2 point. Through the use of linearized equation of motions we have shown how a formation of spacecrafts could be achieved in a real application.

REFERENCES

1. Roberts J. A. *Satellite formation flying for an interferometry mission*. PhD thesis, Cranfield University, 2005.

2. Gill E, Steckling M, and Butz P. Gemini: A milestone towards autonomous formation flying. In *ESTEC, ESA Workshop on On-Board Autonomy*, Noordwijk, October 17-19, 2001.

3. Carpenter K. The stellar imager: a revolutionary large-baseline imaging interferometer at the sun-earth l2 point. In *Proceedings of the SPIE Conference on New Frontiers in Stellar Interferometry*, Glasgow, June 25, 2004.

4. Wallner O. Darwin system assessment study. *Astrium Summary Report, Issue 1*, 12 December, 2006.

5. McQuade F, Ward R, and McInnes C.R. The autonomous configuration of satellite formations using generic potential functions. In *International Symposium, Formation Flying, Missions and Technologies*, Toulouse, October 29-31, 2002.

6. Brooks R. A. A robust layered control system for a mobile robot. *IEEE Journal Of Robotics And Automation*, Vol. 2, No. 1:14–23, 1986.

7. Izzo D, Pettazzi L, and Ayre M. Self-assembly in space using behaviour-based intelligent components. *ESA Internal Report, Issue 2*, 29 June, 2005.

8. Reif J.H. and Wang H. Social potential fields: A distributed behavioral control for autonomous robots. *Robots and Autonomous Systems*, Vol. 27, No. 3:171–194, 1999.

9. Badawy A. and McInnes C. R. Autonomous structure assembly using potential field functions. In *57th International Astronautical Congress*, Seville, October 2-6, 2006.

10. Winfield A, Harper C, and Nembrini J. Towards dependable swarms and a new discipline of swarm engineering. In *SAB Swarm Robotics Workshop*, Santa Monica, July 17, 2004.

11. Jordon D.W. and Smith P. *Nonlinear Ordinary Differential Equations: An Introduction to Dynamical Systems*. Oxford University Press, 1999.

12. Rade L. and Westergren B. *Mathematics Handbook for Science and Engineering*. Studentlitteratur, 1989.

13. D'Orsogna M. R, Chuang Y. L, Bertozzi A. L, and Chayes S. The road to catastrophe: stability and collapse in 2d driven particle systems. *Physical Review Letters*, Vol. 96, No. 10:14302–1, 2006.

14. Weisstein E. W. Wolfram web resource: Cusp catastrophe. *www.mathworld.wolfram.com*, 27/10/2007.

15. McInnes C. R. Vortex formation in swarms of interacting particles. *Physical Review E*, Vol. 75, No. 3:032904, 2007.

16. Wie B. *Space Vehicle Dynamics and Control*. AIAA Educational Series, 1998.

17. Kalman R. E. and Bertram R. E. Control system analysis and design via the second method of lyapunov part i: Continuous systems. *Trans. ASME*, Vol. 82:371–393, 1960.

18. Kalman R. E. and Bertram R. E. Control system analysis and design via the second method of lyapunov part ii: Discrete systems. *Trans. ASME*, Vol. 82:394–400, 1960.

19. LaSalle J. P. The invariance principle in the theory of stability. *NASA Technical Report*, June 23, 1966.